# USE OF STIMULATED BRILLION SCATTERING-PHASE CONJUGATE MIRROR FOR EFFECTIVE MULTI-PASS IMAGING IN TURBULENT FLAMES WITHOUT SPATIAL RESOLUTION DEGRADATION

A Thesis

Presented in Partial Fulfillment of the Requirements for

Graduation with Distinction in the

Department of Mechanical Engineering at

The Ohio State University

By

Dan Marrinan

* * * * *

The Ohio State University

November 2013

# ABSTRACT

Rayleigh and Raman scattering describe the elastic and inelastic scattering of light, respectively, from molecules. Rayleigh scattering is proportional to the number density of the flow and can be used to measure concentrations or temperatures of mixing fluids. Raman scattering is species specific and can be used to measure major species concentration and mixture fraction in combustion systems. However, the signal collected from both Rayleigh and Raman scattering is inherently weak. A retro-reflector is an optic that reflects an incident light beam back along its incoming direction. Thus, in principal, a retro-reflector can increase the collected Rayleigh and Raman signals by "N" times, where "N" is the number of retro-reflections. Typical retro-reflectors used to make high power multipass laser systems degrade the spatial resolution of Rayleigh and Raman measurements because it is not possible to reflect the laser beam back upon itself in environments with strong index of refraction gradients such as those found in combustion systems. A phase conjugate mirror (PCM) can reverse both the propagation direction and phase of an incoming light wave, thus providing the opportunity for near-perfect retro-reflection. This research will be used as a proof-of-concept demonstration showing that the unique characteristics of a PCM can be used to increase the signal for one dimensional Rayleigh scattering imaging in turbulent flames without degrading the spatial resolution. Single pass Rayleigh scattering measurements will be compared to double pass Rayleigh scattering measurements using a conventional mirror and double pass Rayleigh scattering measurements using a PCM. Turbulent combustion flow fields will be used to study the effects of flows with index of refraction gradients. Initial Rayleigh scattering measurements using the PCM will serve as a proof of concept for Raman scattering experiments which are signal limited.

## ACKNOWLEDGMENTS

I would like to thank Dr. Jeffrey Sutton for the opportunity to conduct this undergraduate research project. He has been incredibly helpful and supportive throughout this process. I would also like to thank Frederik Fuest for his assistance and patience while teaching me all of the necessary skills to perform this research. Additionally I would like to thank the other members of TCRL for their advice and assistance during this project. Finally I would like to thank my friends and family for all of their support while I was working on this project.

# TABLE OF CONTENTS

# CHAPTER 1

## RAYLEIGH AND RAMAN SCATTERING

The elastic scattering of light occurs when the scattered light and incident light have the same wavelength. Elastic scattering occurs as a result of the interactions between the electric field of incident light and the electric field of a molecule. Rayleigh scattering is elastic scattering from molecules and Mie scattering is elastic scattering from larger particles. Rayleigh scattering describes the interaction between light and molecules when the wavelength of light is much less than the diameter of the molecule [6].

Rayleigh scattering is the strongest of molecular light scattering techniques. Laser Rayleigh scattering is a nonintrusive combustion diagnostic that uses a laser to produce spontaneous Rayleigh scattering. The ability of a molecule to scatter light elastically is given by its Rayleigh scattering cross section. It is defined as the intensity divided by the irradiance of light scattered for an individual molecule and is given by

$$\sigma_{ri} = \frac{4\pi(n_i-1)^2}{\lambda^4 N_0^2}\sin^2\theta \cdot \frac{3}{3-4\alpha} \tag{1.1}$$

where $n_i$ and $N_0$ are the index of refraction and density at standard temperature and pressure, $\lambda$ is the wavelength of radiation, $\theta$ is the angle between the incident and scattered light, and $\alpha$ is the depolarization ratio. The intensity of light scattered perpendicular to the beam is thus

$$I_{pe} = C_0 I_0 \Omega l N \sum_{i=1}^{j} X_i \sigma_{ri} \tag{1.2}$$

where $I_0$ is the incident light intensity, N is the number density, $X_i$ is the mole fraction of given species and for a given optical setup $C_0$, $\Omega$, l are constants describing collection geometry. Thus the intensity of light scattered is a function of the incident light intensity and the number density of the gas. For a given incident laser energy the scattered intensity can be measured and used to calculate the number density of a gas if the species are known. This number density can be used to determine quantities such as density, temperature, and concentration in combustion environments.

The inelastic scattering of light occurs when scattered light and incident light are of different wavelengths. The inelastic scattering of light from molecules is known as Raman Scattering. Raman scattering describes the excitation of a molecule into a higher vibrational or rotational mode when incident photons transfer energy to a molecule or vice versa. When energy is transferred to a molecule, the scattered light is "Stokes shifted" to lower frequencies. When energy is transferred to a photon the scattered light is "anti-Stokes shifted" to a higher frequency. Shifts in frequency that result from Raman scattering depend on the number of molecules at a particular energy state. Thus Raman scattering spectra are dependent on both the particular species and species number density. Raman scattering spectra can also be used to calculate temperature [6].

Rayleigh scattering cross sections are often three orders of magnitude larger than Raman scattering cross sections for the same species. Thus Rayleigh scattering intensities are much larger than Raman scattering intensities for a given incident laser energy. The high Rayleigh scattering intensities makes it easier to perform Rayleigh scattering measurements with high spatial and temporal resolution and signal-to-noise ratios. However, because the scattered light is at the same frequency for all molecules, Rayleigh scattering is not a species specific diagnostic, in genera [6l. For species-specific measurements (e.g. composition within a flame), Raman scattering is required. However, as mentioned previously, Raman scattering signals are very weak. Thus methods to increase signal collection are highly desired.

# CHAPTER 2

## STIMULATED BRILLOUIN SCATTERING AND PHASE CONJUGATION

Inhomogeneities in the optical properties of a system can cause incident light to be scattered from the particles that make up that system. If the fluctuations in the optical properties of a system are present before interacting with the incident beam the scattering is called spontaneous scattering. When the variations in optical properties are caused by the interaction of the medium and the incident light the scattering is called stimulated scattering. Stimulated scattering tends to scatter a higher percentage of the incoming light than spontaneous scattering. An important method of stimulated scattering is known as stimulated Brillouin scattering. Brillouin scattering is the scattering of light off of acoustic waves.

One method of achieving stimulated Brillouin scattering is through a process known as electrostriction. Electrostriction is the compression of a material in the presence of an electric field. The dipole moment of a molecule in an applied electric field is

$$\boldsymbol{p} = \epsilon_0 \alpha \boldsymbol{E} \tag{2.1}$$

where $\mathbf{p}$ is the dipole moment, $\varepsilon_0$ is the permittivity of free space, $\alpha$ is the polarizability and $\mathbf{E}$ is the applied electric field. From this we can find the energy stored in the polarization of the molecule to be

$$U = -\int_0^E \boldsymbol{p} \cdot d\boldsymbol{E'} = -\frac{1}{2}\epsilon_0 \alpha E^2 \tag{2.2}$$

Finally we can find the force acting on the molecule to be

$$\boldsymbol{F} = -\nabla U = \frac{1}{2}\epsilon_0 \alpha \nabla(E^2) \tag{2.3}$$

Thus if an electric field is applied to a dielectric fluid the dielectric force can cause changes in the density of this fluid [4].

The stimulated Brillouin scattering process begins when the incoming beam of frequency $\omega_1$ spontaneously scattered from thermally excited phonons. The spontaneously scattered light and the incident beam beat together and cause variations in the density of the dielectric fluid via electrostriction as described above. These density variations cause acoustic waves with the Brillouin frequency $\Omega_B$ to form and to travel in the same direction as the oncoming beam. Stimulated Brillouin scattering then occurs when the incident beam scatters from these acoustic waves with the Stokes frequency $\omega_2 = \omega_1 - \Omega_B$. The scattered light, called Stokes radiation, constructively interferes with the incident beam that caused the acoustic waves and thus the amplitude of the scattered light and acoustic waves continue to grow. A diagram of the stimulated Brillouin scattering process is shown below in Figure 2.1.

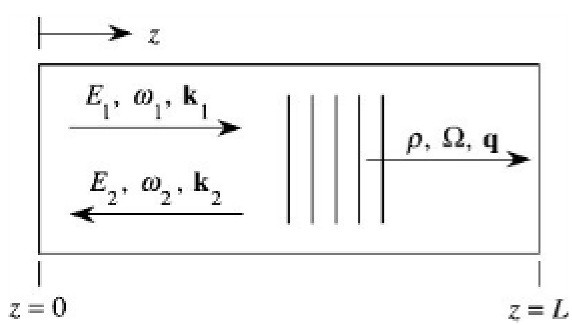


Figure 2.1 Diagram of Brillouin Scattering Process [4]

The scattered Stokes radiation from stimulated Brillouin Scattering is a phase conjugate of the incident beam. This means that both the propagation direction and phase variation of the incident beam are reversed. A comparison between a conventionally reflected beam and a phase conjugated beam is shown below in Figure 2.2.

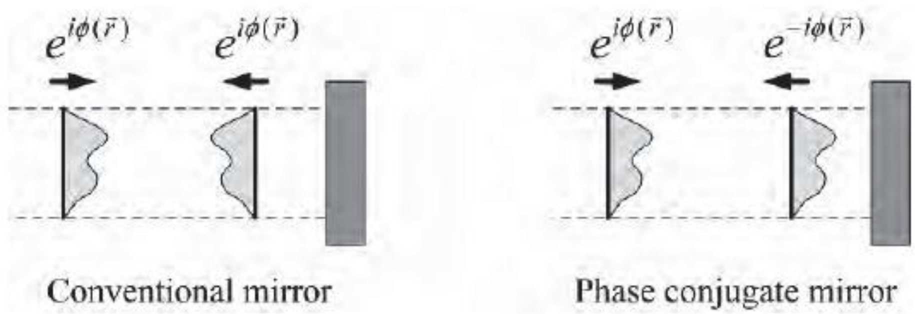


Figure 2.2: Demonstration of a phase conjugate beam [5]

When a beam is passed through a boundary between two differing index of refractions the wavefront is distorted. The wavefront of a beam reflected from a conventional mirror will be distorted twice when it passes back through the index of refraction boundary. The reversal of the phase in phase conjugation causes the distortions of the original pass to be undone when the beam travels back through the index of refraction boundary.

The intensity of the Stokes radiation is dependent on the intensity of the incoming beam. As mentioned earlier, when the stimulated Brillouin scattering process first begins the Stokes radiation and the acoustic waves amplify each other. Thus the acoustic waves that best match the incident wavefront will be amplified while those that do not will continue to have small amplitudes. Thus the acoustic waves that form during stimulated Brillouin scattering match the incident wave front and scatter a phase conjugate of the incident beam.

# CHAPTER 3

# POLARIZATION OF LIGHT

Visible light is a special case of electromagnetic radiation. Electromagnetic radiation is energy released by an accelerating charged particle. Typically when energy is imparted to the atom of a light source it causes an electron to oscillate about its equilibrium position within the atom and emit an electromagnetic wave. All electromagnetic fields must obey Maxwell's equations. By manipulating these laws one can show that both electric and magnetic fields obey the wave equation. Maxwell's equations also dictate that the electric field $\boldsymbol{E}$ and the magnetic field $\boldsymbol{H}$ are mutually orthogonal and oscillate sinusoidally in a plane perpendicular to the wave vector $\boldsymbol{k}$ which points in the direction of propagation [1].

Using the principle of superposition we can model the electric field of an electromagnetic wave as the sum of two orthogonal waves,

$$\boldsymbol{E} = Re\{(\boldsymbol{E}_x + \boldsymbol{E}_y)e^{i(kz-\omega t)}\} = Re\{(\boldsymbol{x}ae^{-i\phi_x} + \boldsymbol{y}be^{-i\phi_y})e^{i(kz-\omega t)}\}, \tag{3.1}$$

where $\boldsymbol{x}$ and $\boldsymbol{y}$ are orthogonal unit vectors in the wave plane and z is the direction of propagation. The tip of the electric field vector traces out a shape on the wave plane. If $a$ and $b$ have different magnitudes and $\phi_x$ and $\phi_y$ are not equal then this shape is an ellipse and the electromagnetic wave are said to be "elliptically" polarized. If $a$ and $b$ are equal and $\phi_x$ and $\phi_y$ differ by $\pi/2$ this shape is a circle and the wave is said to be "circularly" polarized. If $\phi_x = \phi_y$ or $\phi_x = -\phi_y$ this shape is a line and the wave is said to be linearly polarized. It is also possible for $a$ and $b$ to be random functions of time in which case the wave is said to be unpolarized [1].

A beam of light incident on a plane can have an s component of polarization and p component of polarization. P polarized light oscillates in the plane that contains the normal vector to the plane of incidence. S polarized light oscillates orthogonally to the plane that contains the normal vector to the plane of incidence. This relationship can be seen below in Figure 3.1.

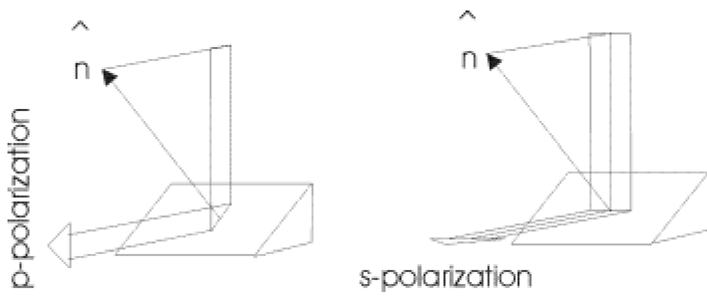


Figure 3.1: S vs. P Polarization [2]

In the laboratory S polarization is parallel to the ground so S polarization is called “horizontal” polarization and P polarization is called “vertical” polarization.

The electric displacement vector $\boldsymbol{D}$ is defined as

$$\boldsymbol{D} = [\epsilon]\boldsymbol{E}, \tag{3.2}$$

where $\boldsymbol{E}$ is the electric field, and $[\epsilon]$ is the dielectric permittivity tensor. $\boldsymbol{D}$ describes the electric field’s interaction with the material in which it is located. Once $[\epsilon]$ has been diagnalized the values $\epsilon_{xx}$, $\epsilon_{yy}$, and $\epsilon_{zz}$ are known as the principal dielectric constants of the material and describe how the field interacts with a material along each of its principal axes [1]. An isotropic dielectric material has the same value of ε in every direction. This gives an isotropic dielectric material a uniform index of refraction in every direction. The index of refraction of a material measures the speed that light travels through this medium relative to the speed that light travels through a vacuum. Snell’s law says that at the boundary between two materials with different indices of refraction

$$\frac{\sin\theta_0}{\sin\theta_1} = \frac{n_1}{n_0} \tag{3.3}$$

where $\theta_0$ is the angle between the incident ray and the normal to the face, $\theta_1$ is the angle between the outgoing ray and the normal to the face, the ns are the index of refraction of each [2].

A uniaxial anisotropic material has a fixed "optical axis" for one of its principal axes. The other two axes though perpendicular to each other are free to rotate about the optical axis [1]. When a beam of incident light hits the face of an anisotropic material and creates two transmitted beams. Thus anisotropic materials are also called birefringent because they cause two beams to be refracted [1].

A birefringent, uniaxial material which causes the two refracted beams to travel along the same path but at different velocities is known as a retardation plate. The ordinary beam oscillates along the optical axis and has an index of refraction of $n_o$. The extraordinary beam oscillates along an within the wave plane that is perpendicular to the optical axis and has an index of refraction of $n_e$. This can be seen in Figure 3.2. The phase difference between the ordinary and extraordinary rays is given by

$$\delta = 2\pi N = \pm\frac{2\pi d(n_e - n_o)}{\lambda}, \tag{3.4}$$

where $N$ is the fraction of a wavelength retarded, $d$ is the thickness of the retardation plate, and $\lambda$ is the wavelength of light. Thus $N$ = ½ for a half-wave ($\lambda/2$) plate [3]. Thus to rotate a linear polarized beam by a specified angle one must pass it through a $\lambda/2$ plate with its optical axis at half of the desired angle relative to the polarization to the beam [2].

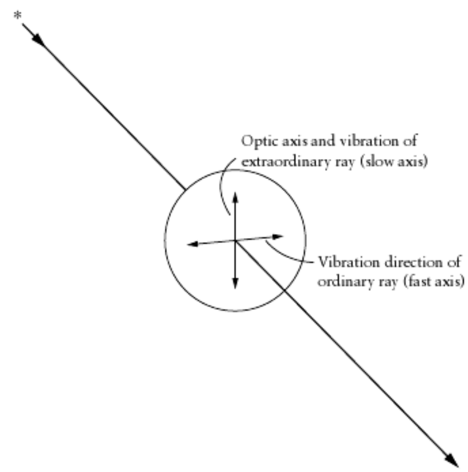


Figure 3.2: Retardation Plate [3]

Crystal quartz polarization rotators can also rotate the polarization of a beam. A rotator rotates a beam's polarization by a fixed amount that is proportional to the rotator's thickness. Unlike wave retarders, the relative angle between the rotator and the polarization of the incident like does not impact the rotation of the polarization. A rotator also rotates the polarization in the opposite direction when passing through the rotator in the opposite direction [2].

A Rochon prism can be used as a polarizing beam splitter cube. It has two triangular prisms glued together to form a cube shape. The material that makes up the cube is birefringent and uniaxial. Thus if the incident beam is at horizontal polarization it travels straight through the beam splitter cube. If the beam is at vertical polarization the beam refracts from the angled surface inside the cube where the prisms meet [2].

# CHAPTER 4

# METHODS

In this chapter, we investigate the use of a double pass stimulated-Brillion scattering phase conjugate mirror to increase the signal collected from Rayleigh scattering experiments in a turbulent flame without the degradation of spatial resolution. A conventional single pass experimental set up was compared to double pass experimental set ups utilizing a conventional mirror and a phase conjugate mirror. Images were taken in air and in a turbulent flame. The increase in signal and the relative beam width of all three experiments could then be compared when there were index of refraction gradients and no index of refraction gradients in the flow.

A frequency doubled Nd:YAG laser was used to generate a 10-ns long, horizontally-polarized, 532-nm laser pulse at a rate of 10 Hz. The laser was reflected into the test section using a 45° mirror. It then passed through a polarized beam splitter cube, a 45° quartz rotator, a $\lambda/2$ waveplate, and then focused down into the test section using a 750 mm focal length lens. The quartz rotator and waveplate changed the polarization so that the beam was vertically-polarized as it traveled through the test section. After the test section the beam was recollimated using a 750 mm focal length lens and then focused down using a 300 mm lens. For the single pass measurements a beam dump was placed after the 300 mm lens to determine the beam energy that interacted with the gas in the test section.

For the double-pass measurement using the PCM as a retroreflector the beam was focused down into the PCM by the 300-mm lens mentioned above. The beam was then reflected back through the 300- mm lens, 750-mm lens, test section, 750-mm lens, waveplate, and quartz rotator. As mentioned in previously the polarization shift of a quartz rotator is directionally dependent while the polarization shift of a waveplate is not. Thus after traveling back through the optics for the second time the beam remained vertically-polarized. When the beam reached the polarized beam splitter cube it was reflected into a power meter where the reflected energy was measured. When the mirror was swapped for the PCM the rest of the setup was the same except the 300-mm lens was removed so that the beam was not focused down onto the face of the mirror.

For all three setups a CCD camera was placed perpendicular to the direction of the beam propagation next to the test section. A lens with an f-number of 2 was used to focus the images on the beam when it traveled above the nozzle within the test section. An air coflow was used for all measurements to ensure that no dust particles would be in the beam path over the test section. A target with markings ¼” apart was used to measure the resolution of the images taken. The resolution for all images was 9.82 microns per pixel. Images were taken for all three set ups in air and again at an x/d of 30 in an SLR flame. The three experimental set ups are shown in Figures 4.1, 4.2, and 4.3 respectively.

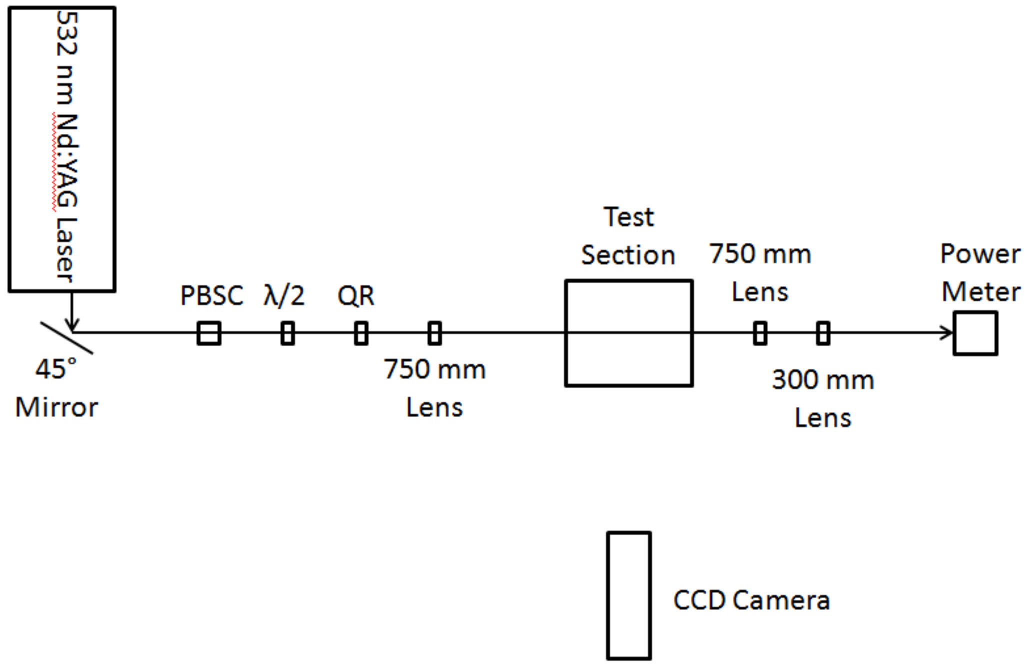


Figure 4.1: Single Pass Experimental Setup

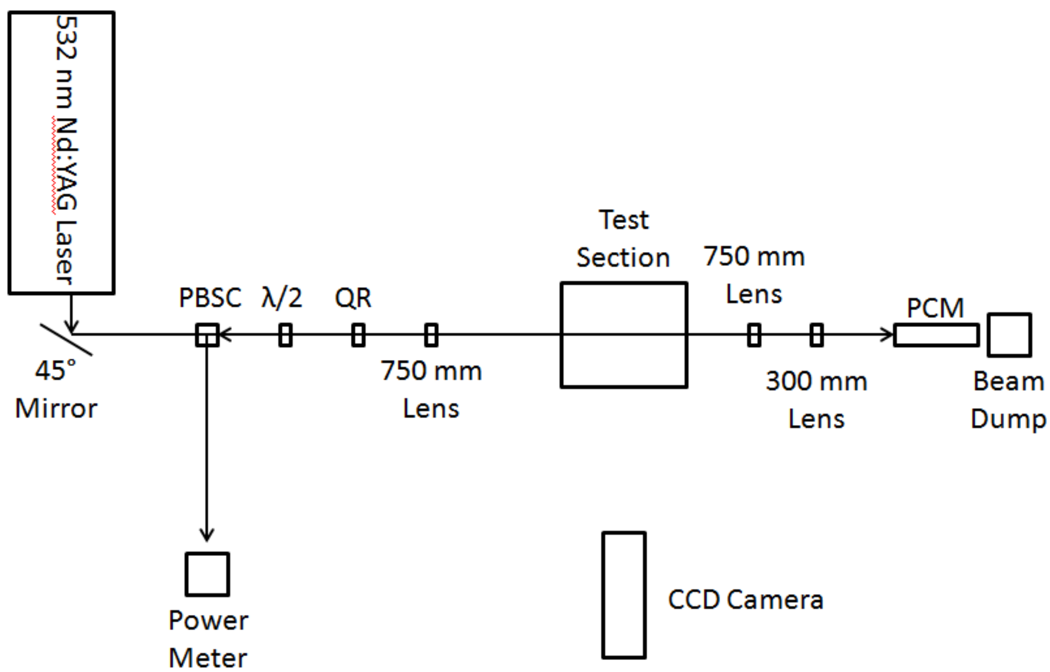


Figure 4.2: Double Pass PCM Experimental Setup

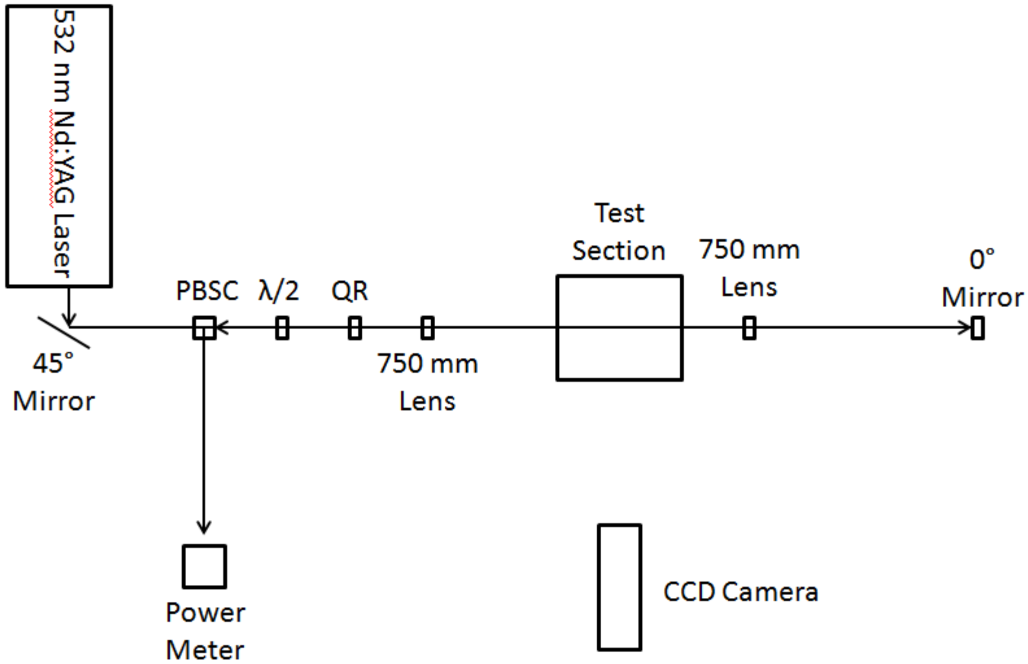


Figure 4.3: Double Pass Mirror Experimental Setup

## CHAPTER 5

## RESULTS

The images displayed in Figure 5.1 show the average beam profile, as interpreted from the Rayleigh scattering images, for the single pass, double pass PCM, and double pass mirror measurements taken in air. Images acquired in air represent a “control” case, where no index-of-refraction gradients are expected. In this manner it is expected that the single-pass, double-pass mirror, and double-pass PCM cases result in similar spatial resolution. The average beam profile for the three experimental setups can be seen in Figure 5.2. The signal collected for the conventional mirror was 80% larger than that of the single pass measurement. The signal collected for the PCM was 50% larger than that of the single pass measurement. Histograms of the beam width for the image sets corresponding to each experimental set up can be seen in Figure 5.3. The average beam width for the single pass measurement was 152 microns. The average beam width for the double pass mirror images was 196 microns. This is an increase of 35 microns or 22% from the single pass measurement. The average beam width for the double pass PCM images was 181 microns. This is an increase of 29 microns or 19% from the single pass measurement. Histograms of the displacement of the peak location for the image sets corresponding to each experimental set up can be seen in Figure 5.4.

The three experimental setups behaved mostly as expected in air. Since there were no index of refraction gradients, no beam steering effects were observed. The average images seen in Figure 5.1 and the beam profiles seen in Figure 5.2 have the same general shape. There was an increase in signal in both double pass measurements relative to the single pass measurement but only a slight increase in beam width. The main anomaly seen in this data was that only 50% of the incident energy was reflected back through the test section by the PCM. Future work will explore the lower efficiency of the SBS PCM retro-reflection

The images shown in Figure 5.5 display the average beam for the single pass, double pass PCM, and double pass mirror measurements taken in the turbulent flame. The average beam profile for the three experimental setups can be seen in Figure 5.6. The signal collected for the conventional mirror was 80% larger than that of the single pass measurement. The signal collected for the PCM was 50% larger than that of the single pass measurement. Histograms of the beam width for the image sets corresponding to each experimental set up can be seen in Figure 5.7. The average beam width for the single pass measurement was 182 microns. The average beam width for the double pass mirror images was 282 microns. This is an increase of 100 microns or 55% from the single pass measurement. The average beam width for the double pass PCM images was 189 microns. This is an increase of 7 microns or 4% from the single pass measurement. Histograms of the displacement of the peak location for the image sets corresponding to each experimental set up can be seen in Figure 5.8.

A single image from the double pass mirror set up is shown in Figure 5.9. It showcases the beam steering that results from index of refraction gradients within the flame. For this particular case the index-of- refraction gradients completely separated the reflected beam from the incident beam. The three experimental setups behaved mostly as expected in the flame. Figures 5.5, 5.6, and 5.7 show significant widening of the beam in the double pass mirror experimental set up due to beam steering effects. They also show that the beam width of the double pass PCM experimental set up was negligible relative to the single pass measurement.

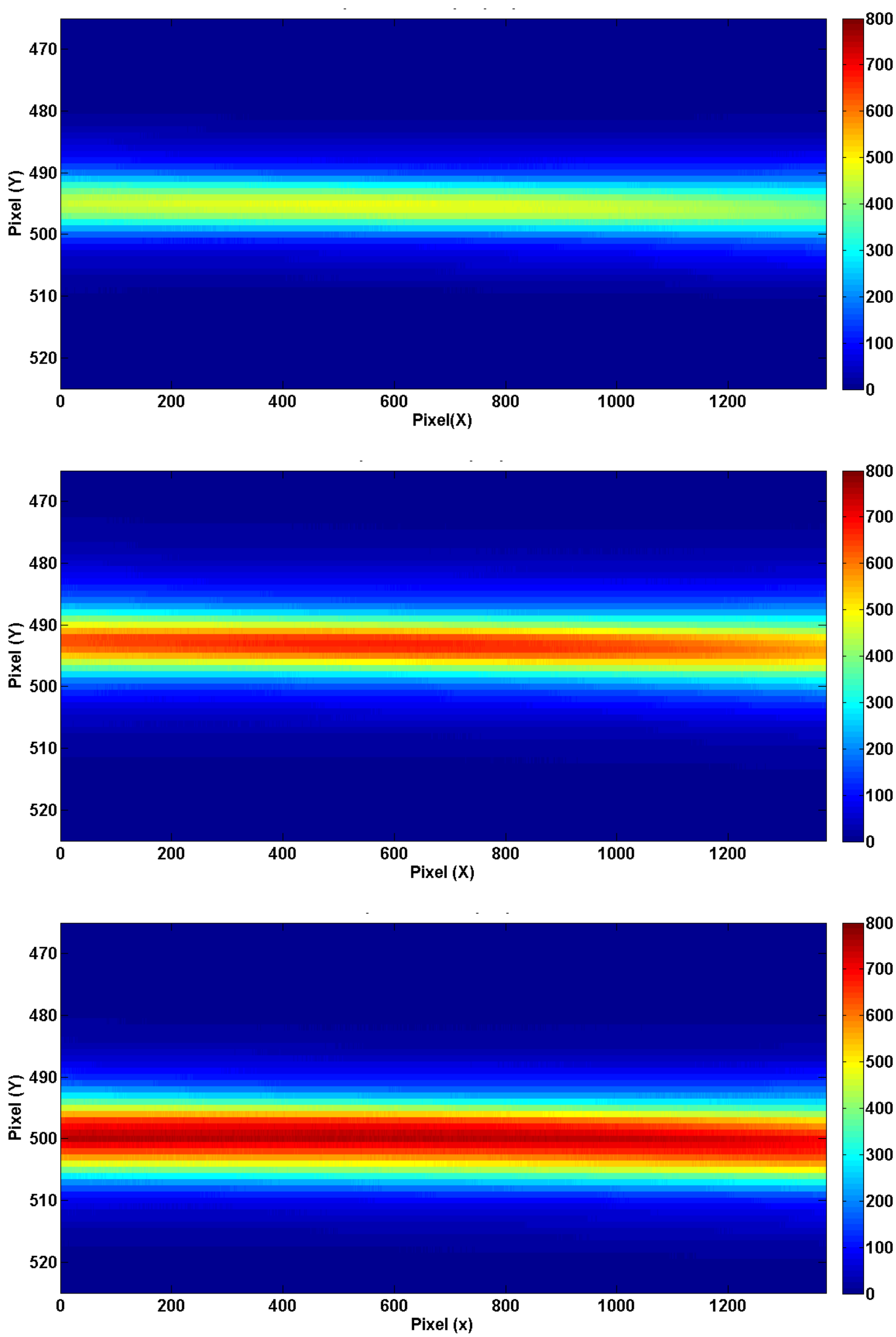


Figure 5.1: Average Rayleigh Scattering Images in Air Using Single Pass, Double Pass PCM, and Double Pass Mirror Experimental Setups

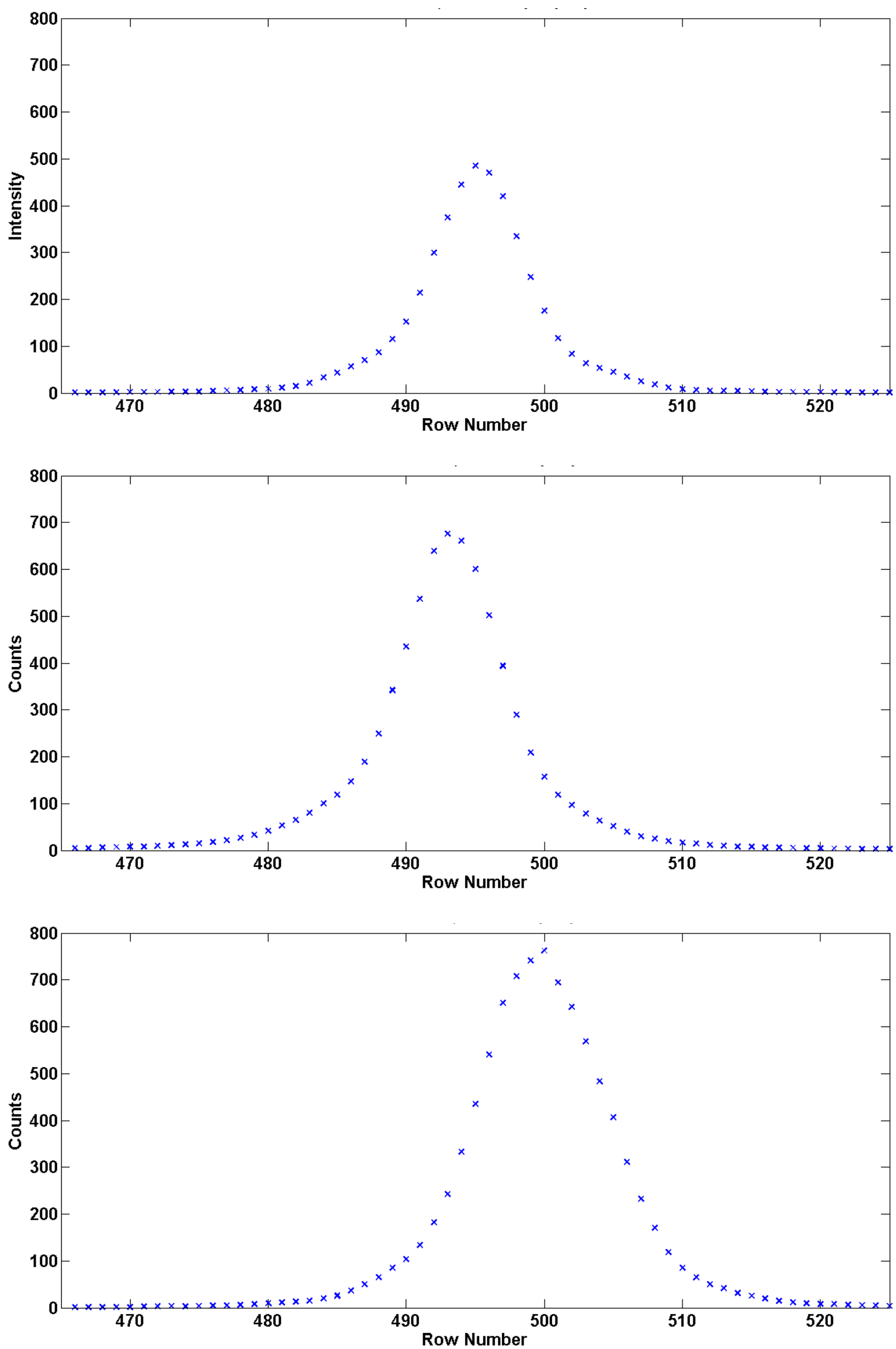


Figure 5.2: Average Beam Profiles of Rayleigh Scattering Images in a Air Using Single Pass, Double Pass PCM, and Double Pass Mirror Experimental Setups

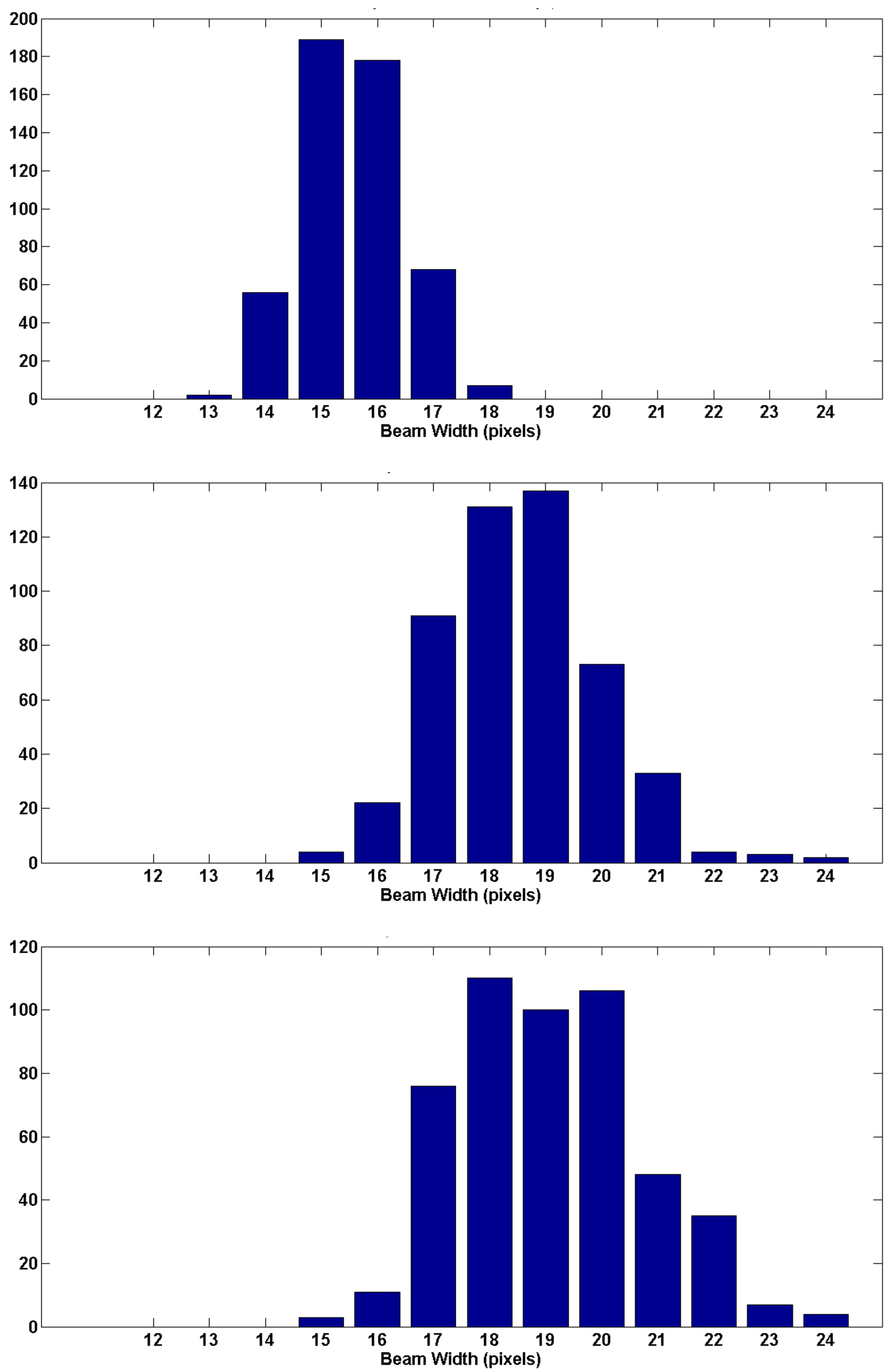


Figure 5.3: Histograms of Beam Width of Rayleigh Scattering Images in a Air Using Single Pass, Double Pass PCM, and Double Pass Mirror Experimental Setups

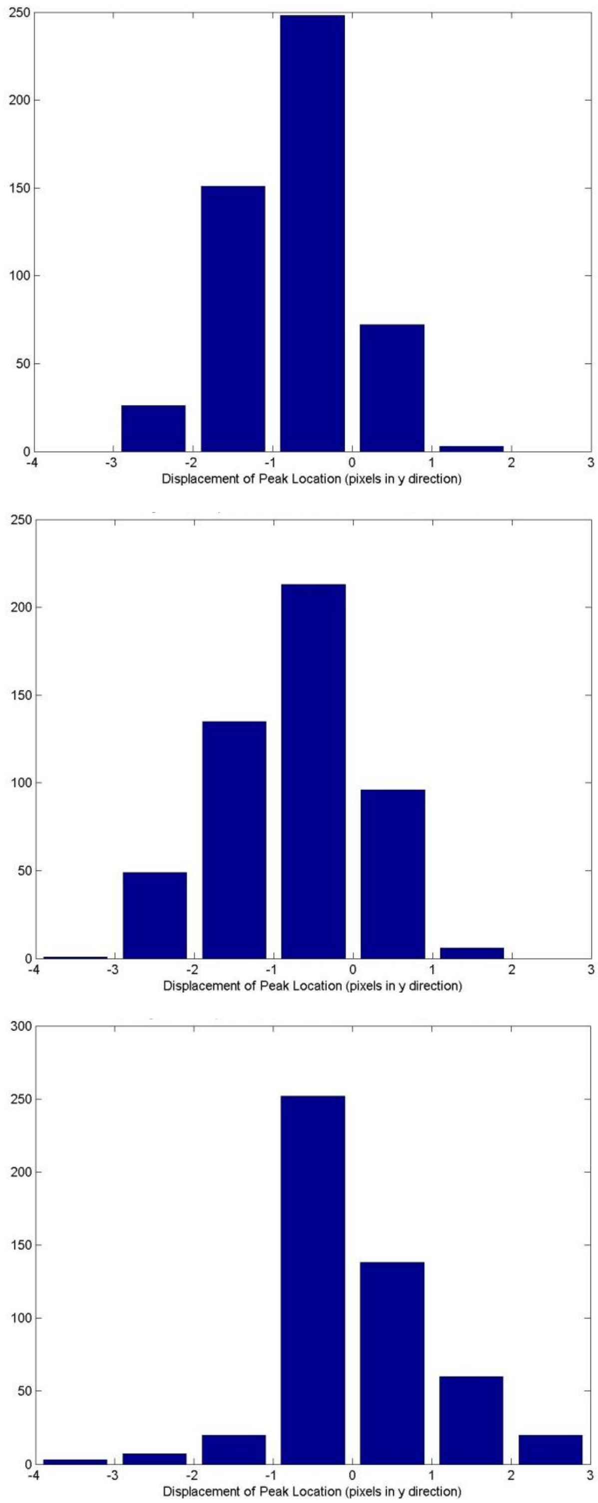


Figure 5.4: Histogram of Y Displacement of Center of Beam from Average Image Location in a Air using Single Pass, Double Pass PCM, and Double Pass Mirror Experimental Setups

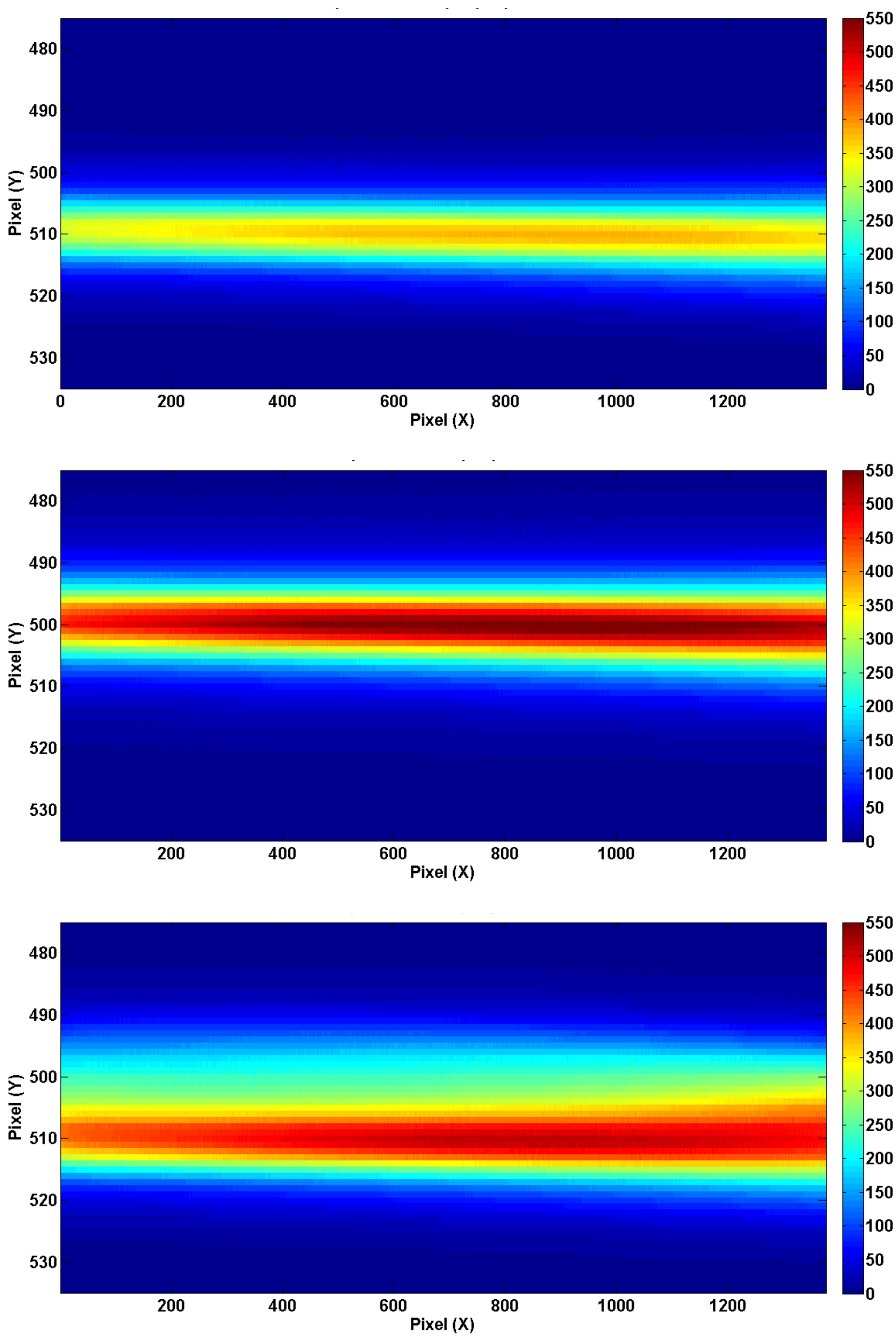


Figure 5.5: Average Rayleigh Scattering Images in a Flame Using Single Pass, Double Pass PCM, and Double Pass Mirror Experimental Setups

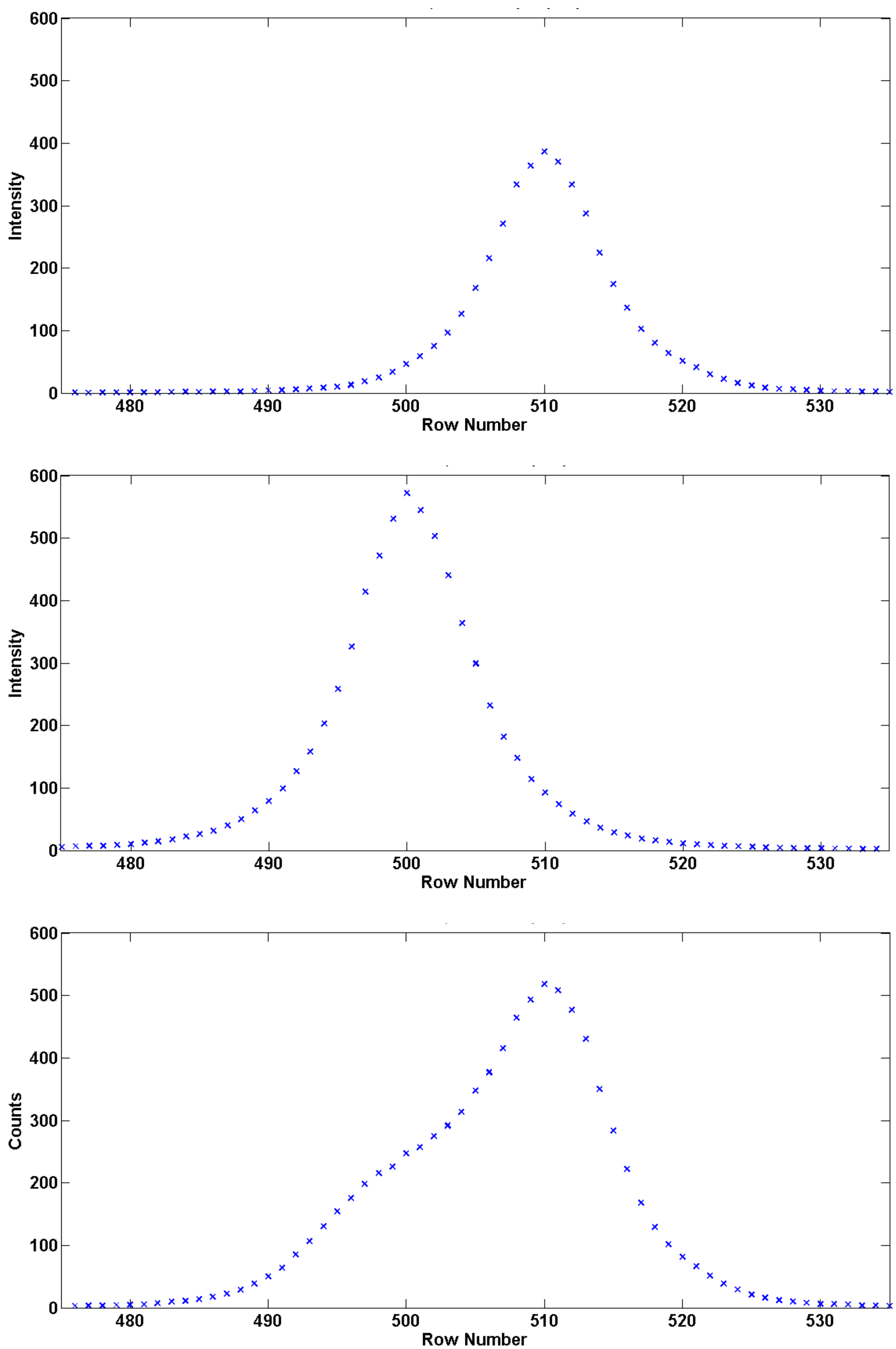


Figure 5.6: Average Beam Profiles of Rayleigh Scattering Images in a Flame Using Single Pass, Double Pass PCM, and Double Pass Mirror Experimental Setups

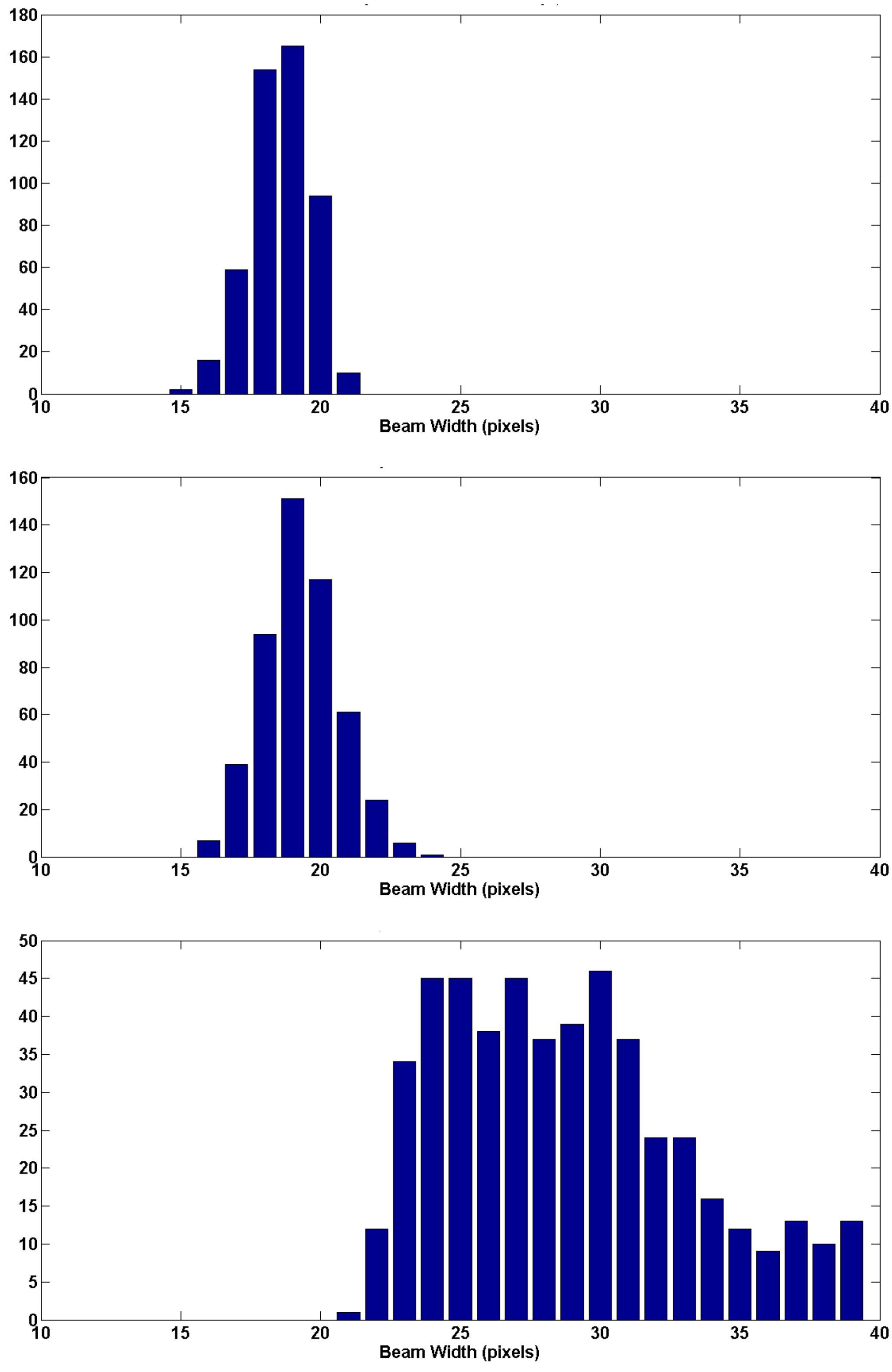

Figure 5.7: Histograms of Beam Width of Rayleigh Scattering Images in a Flame Using Single Pass, Double Pass PCM, and Double Pass Mirror Experimental Setups

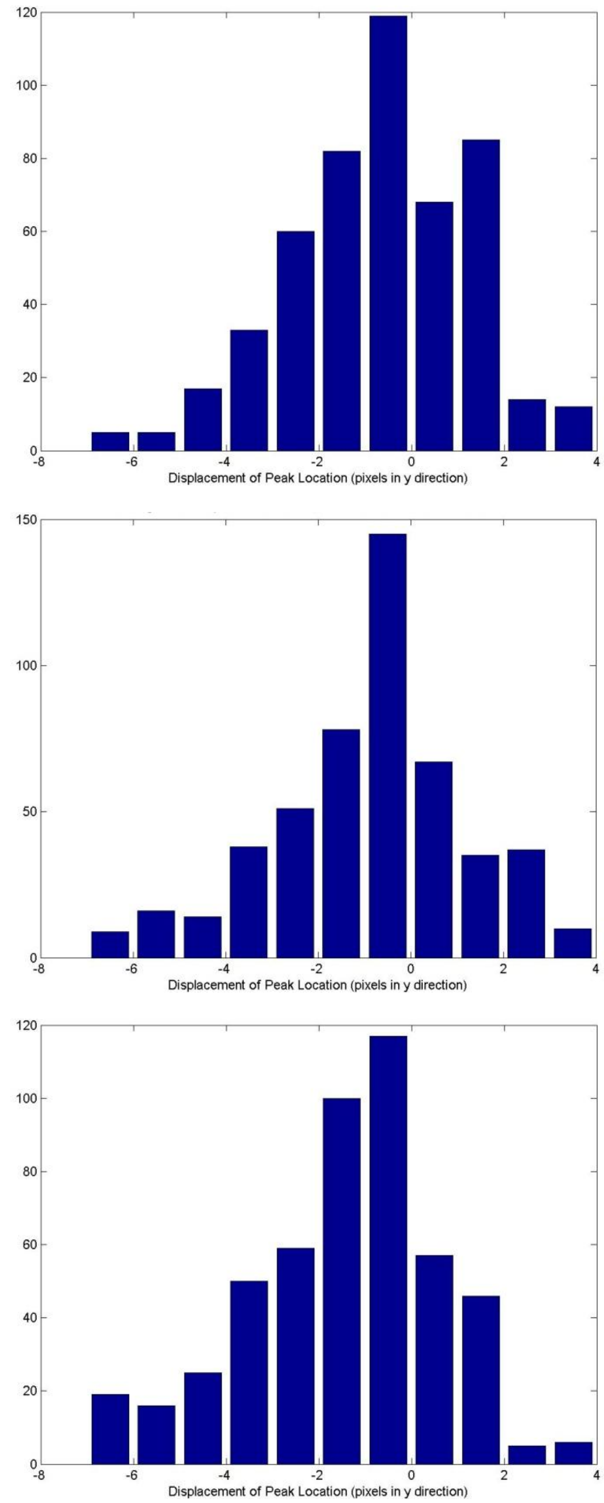


Figure 5.8: Histogram of Y Displacement of Center of Beam from Average Image Location in a Flame using Single Pass, Double Pass PCM, and Double Pass Mirror Experimental Setups

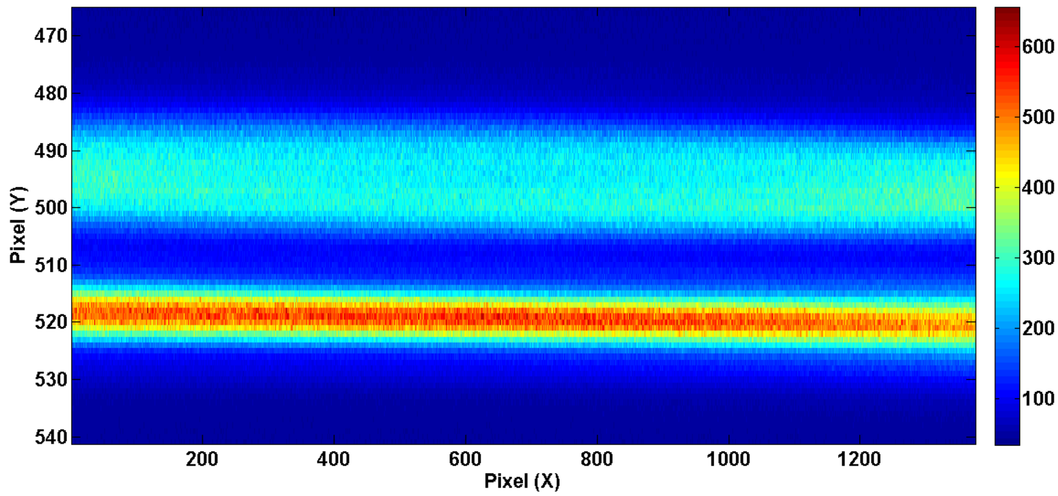


Figure 5.9: Rayleigh Scattering Image Showing Separated Beams in a Flame Using the Double Pass Mirror Experimental Setup

# CHAPTER 6

## CONCLUDING REMARKS

- The SBS PCM successfully increased signal without significantly degrading the spatial resolution of a Rayleigh scattering image within a turbulent flame.

- Measured reflectivity for a conventional mirror was higher than for the PCM but the mirror suffered degradation of spatial resolution in the flame due to beam steering effects.

- Non-reflected energy is not measureable after PCM, but there is an unknown loss of energy or energy transfer mechanism within the system

- In the future Raman scattering measurements will be made with a similar experimental setup to test the SBS PCM retroreflection in systems suffering from low scattering and low signal-to-noise.

## REFERENCES

[1] Chartier, G., 2005, "Introduction to Optics," Springer.

[2] Williamson Ray, 2005, *Polarization Optics Tutorial: Polarizers, Waveplates, Rotators, and Lyot Filters*.

[3] Bass, M., 2009, Handbook of Optics Volume I Geometrical and Physical Optics, Polarized Light, Components and Instruments," McGraw-Hill Professional.

[4] Boyd, R., 2008, "Nonlinear Optics Robert Boyd," Academic Press.

[5] Kong, H.J., 2010, *Stimulated Brillouin Scattering Phase Conjugate Mirror and its Application to Coherent Beam Combined Laser System Producing a High Energy, High Power, High Beam Quality, and High Repetition Rate Output*, Advances in Lasers and Electro Optics.

[6] Zhao, F.Q., 1993,*The Applications of Laser Rayleigh Scattering to Combustion Diagnostics*, Progress in Energy and Combustion Science, v19.